Tunable spin-polarized edge transport in inverted quantum-well junctions

Dimy Nanclares,[1] Leandro R. F. Lima,[2] Caio H. Lewenkopf,[2] and Luis G. G. V. Dias da Silva[1]
[1]*Instituto de Física, Universidade de São Paulo, C.P. 66318, 05315-970 São Paulo, SP, Brazil*
[2]*Instituto de Física, Universidade Federal Fluminense, 24210-346 Niterói, Brazil*
(Received 12 July 2017; published 4 October 2017)

Inverted HgTe/CdTe quantum wells have been used as a platform for the realization of two-dimensional topological insulators, bulk insulator materials with spin-helical metallic edge states protected by time-reversal symmetry. This paper investigates the spectrum and the charge transport in HgTe/CdTe quantum well junctions both in the topological regime and in the absence of time-reversal symmetry. We model the system using the Bernevig-Hughes-Zhang effective Hamiltonian and compute the transport properties using recursive Green's functions with a finite differences' method. Specifically, we have studied the material's spatially resolved conductance in a setup with a gated central region, forming monopolar (n-n'-n) and heteropolar (n-p-n, n-TI-n) double junctions, which have been recently realized in experiments. We find regimes in which the edge states carry spin-polarized currents in the central region even in the presence of a small magnetic field, which breaks time-reversal symmetry. More interestingly, the conductance displays spin-dependent, Fabry-Perót-like oscillations as a function of the central gate voltage producing tunable, fully spin-polarized currents through the device.

DOI: 10.1103/PhysRevB.96.155302

I. INTRODUCTION

The role of topology in the properties of electronic systems has gained renewed attention over the last decade with the discovery of several materials that support topologically protected surface and edge states, dubbed topological insulators (TIs) [1–3]. Particular attention has been given to two-dimensional (2D) topological insulators, where the quantum spin Hall (QSH) effect [4] allows for edge electron transport through spin-polarized helical edge states. The theoretical proposal [5] and later observation [6] of the QSH effect in HgTe/CdTe quantum wells has triggered intense activity in the study of these systems.

The electronic current in 2D topological insulators is carried by edge states protected by time-reversal symmetry (TRS). In the absence of TRS, backscattering between the edge modes becomes allowed and the gaplessness of the edge states is no longer guaranteed. It has been argued [6] that even a small magnetic field is sufficient to open a gap in the edge states, thereby suppressing edge transport in 2D topological insulators. The argument supporting this view comes from the early experiments [6] on HgTe/CdTe quantum wells, which show that the magnetoconductance shows a cusplike feature at zero field, quickly decaying as the field increases. Such behavior, however, can only be accounted for when a rather strong disorder (of the order of the bulk gap) [7] combined with TRS breaking is considered. In addition, dephasing can also be a factor as it has been argued that the resilience of edge transport against dephasing induced by inelastic scattering is weaker as compared to quantum Hall chiral states [8,9].

In many situations, however, breaking TRS does not imply a suppression of edge transport channels in these systems. Several theoretical studies [10–16] as well as experimental evidence [17–19] point to a scenario where edge transport in HgTe/CdTe quantum wells (QWs) is quite relevant up to magnetic fields of a few Tesla. For instance, theory predicts [11,13,14] a transition from helical QSH to chiral QHE edge states at a critical field of a few Tesla.

A recent theoretical study on HgTe/CdTe QWs has shown that for small system sizes the edge states remain unaffected by a combination of moderate disorder and weak magnetic fields [20]. The transport properties change in long samples when considering charge puddles [20]. This kind of disorder and the corresponding local potential fluctuations have been extensively studied in graphene systems [21–23]. It has been found that charge puddles give rise to a disordered landscape of p-n junctions that are key to understand the low-energy electronic transport in realistic graphene samples [24–26].

Recent theoretical [27–29] and experimental [19,30,31] works have studied the transport properties of heteropolar lateral junctions in HgTe/CdTe QWs in the inverted regime. Some experiments [19,31] investigate electronic transport through double junction systems by applying a gate voltage V_g in the central region of a HgTe quantum-well Hall bar. By varying V_g, the system can be tuned from an n-n'-n type junction (Fermi energy lying in the electronlike states of the junction) to n-p-n (Fermi energy lying in the holelike states of the junction). When V_g is tuned close to the charge neutrality point, $V_g = V_g^{\mathrm{CN}}$, the Fermi energy lies near the gap of the central region and the transport across the junction is expected to be dominated, in the absence of magnetic field, by QSH edge states (n-TI-n).

The results presented in Ref. [19] show that, in the presence of a strong perpendicular magnetic field ($B \gtrsim 7$ T) the system enters the quantum Hall regime. The longitudinal conductance displays plateaus consistent with those expected for graphene junctions in the QHE regime [32,33]: $2e^2/h$ in a monopolar n-n'-n junction ($V_g \gg V_g^{\mathrm{CN}}$) and $e^2/2h$ in the bipolar n-p-n junction ($V_g \ll V_g^{\mathrm{CN}}$). In the n-TI-n configuration ($V_g \approx V_g^{\mathrm{CN}}$), a nonquantized conductance value was measured. More intriguingly, well-defined conductance plateaus have not been observed for weaker magnetic fields [19]. This regime has no clear interpretation yet, calling for further theoretical investigation.

With this motivation, we present a simplified model to describe the weak field limit (non-QHE regime) of HgTe/CdTe

QW junctions. We compute the transport properties of pristine HgTe/CdTe QWs and homopolar and heteropolar double junctions by combining a discrete model Hamiltonian with the recursive Green's functions method (RGF) [34]. For concreteness, we consider the Bernevig-Hughes-Zhang (BHZ) model [5] in the presence of a perpendicular magnetic field [14,35]. Our work extends and complements previous theoretical studies that have addressed the electronic transport in TI-double junctions in the absence of external magnetic fields [28,29].

We calculate the space-resolved transmission across different types of junctions (n-n'-n, n-edge-n, n-p-n) as a function of a gate voltage V_g applied at the system central region and of an external magnetic field. The latter is believed to destroy the topological protection, since it allows for backscattering in the spin-polarized edge states. Interestingly, our results show that, for fields up to a few Tesla, there is always a range of V_g where edge transmission in the central region dominates the transport properties. We refer to this configuration as an n-edge-n junction. We show that some of the transport features of the studied n-TI (or p-TI) junctions bear similarities with the case of graphene junctions where the transmission to a region where the transport is forbidden can be understood in terms of snakelike states at the interface [36,37].

One of our main results is that, in an n-edge-n junction, the combined effect of quantum interference from reflection at the junction barriers and edge-state backscattering due to the breaking of TRS creates a spin-dependent Fabry-Pérot pattern in the transmission amplitudes. These gate-controlled oscillations are strong enough to provide fully spin-polarized currents across the junction.

The paper is organized as follows. In Sec. II we present the BHZ model used to describe the HgTe junctions and discuss the recursive Green's functions approach employed to investigate the local currents in the system. Our numerical results are presented in Sec. III, where we study the effect of a perpendicular external magnetic field on the transport properties across the junction. Finally, we present our concluding remarks in Sec. IV.

II. MODEL AND METHODS

We describe the physical properties of HgTe/CdTe QWs at low energies and zero magnetic field using the four-band BHZ Hamiltonian [5]

$$\hat{H} = \mathcal{C}\mathbf{1} + \mathcal{M}\Gamma_5 - \frac{(\mathcal{D}\mathbf{1} + \mathcal{B}\Gamma_5)}{\hbar^2}\left(\hat{p}_x^2 + \hat{p}_y^2\right) - \frac{\mathcal{A}\Gamma_1}{\hbar}\hat{p}_x + \frac{\mathcal{A}\Gamma_2}{\hbar}\hat{p}_y, \tag{1}$$

where Γ_1, Γ_2 and Γ_5 are 4×4 matrices spanning the basis $\{|E\uparrow\rangle,|H\uparrow\rangle,|E\downarrow\rangle,|H\downarrow\rangle\}$, which can be expressed in terms of Pauli matrices σ_j, namely

$$\Gamma_1 = \begin{pmatrix} \sigma_x & 0 \\ 0 & -\sigma_x \end{pmatrix}, \quad \Gamma_2 = \begin{pmatrix} -\sigma_y & 0 \\ 0 & -\sigma_y \end{pmatrix}, \quad \Gamma_5 = \begin{pmatrix} \sigma_z & 0 \\ 0 & \sigma_z \end{pmatrix}, \tag{2}$$

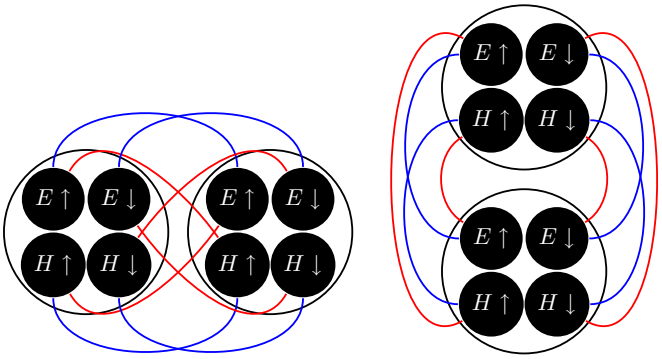

FIG. 1. Sketch of the hopping matrix element structure in our discretized model. Each site (large circle) has a fourfold orbital structure with states (black circles) of the basis $\{|E\uparrow\rangle,|H\uparrow\rangle,|E\downarrow\rangle,|H\downarrow\rangle\}$. The lines represent the nonvanishing hoppings between states that belong to different sites. No hopping between states in the same site is allowed. Left: Hoppings between orbitals belonging to the sites at (n,m) and $(n+1,m)$. Right: Hoppings between (n,m) and $(n,m+1)$.

and $\mathbf{1}$ is the identity. The numerical parameters $\mathcal{A},\mathcal{B},\mathcal{C},\mathcal{D}$ depend on system properties such as the QW thickness.

We caution that the indices "↑" and "↓" indicate degenerate Kramers pairs related by TRS in the low-energy effective model obtained from the original $\mathbf{k}\cdot\mathbf{p}$ six-band model for HgTe near the Γ ($\mathbf{k}=0$) point [5]. In this sense, the latter are not pure spin $1/2$ states since the H states carry contributions from p-type heavy-hole bands with spin $J_z = \pm 3/2$. However, to a good approximation, these states represent spin-$1/2$ states related by TRS [12,14] and we will treat them as such in the present paper. In addition, since our focus will be on the TRS-broken regime, we will neglect TRS-preserving perturbations such as inversion-breaking [16] and Rashba spin-orbit coupling [28,29] terms that give rise to coupling between the spin-up and the spin-down sectors [38].

The numerical calculation of the QW transport properties follows the prescription of Ref. [14]. We discretize the four-component spinor $\Psi(x,y)$ in a square lattice of spacing a in both x and y directions. The spinor $\Psi(x,y)$ becomes $\Psi_{n,m}$ where $x = na$ and $y = ma$ and n and m are integer. Figure 1 shows the orbital structure of the hopping matrix elements. We note that the hopping terms between electron and hole states are nonzero only if the spin projection is preserved.

Using two and three points derivatives for the momenta discretization

$$\begin{aligned} p_x\Psi(x,y) &\to -\frac{i\hbar}{2a}\left(\Psi^m_{n+1} - \Psi^m_{n-1}\right), \\ p_x^2\Psi(x,y) &\to -\frac{\hbar^2}{a^2}\left(\Psi^m_{n+1} - 2\Psi^m_n + \Psi^m_{n-1}\right), \\ p_y\Psi(x,y) &\to -\frac{i\hbar}{2a}\left(\Psi^{m+1}_n - \Psi^{m-1}_n\right), \\ p_y^2\Psi(x,y) &\to -\frac{\hbar^2}{a^2}\left(\Psi^{m+1}_n - 2\Psi^m_n + \Psi^{m-1}_n\right), \end{aligned} \tag{3}$$

the eigenvalue problem $\hat{H}\Psi(x,y) = E\Psi(x,y)$, becomes

$$E\Psi^m_n = H^{m,m}_{n,n}\Psi^m_n + H^{m,m}_{n,n-1}\Psi^m_{n-1} + H^{m,m}_{n,n+1}\Psi^m_{n+1} + H^{m,m-1}_{n,n}\Psi^{m-1}_n + H^{m,m+1}_{n,n}\Psi^{m+1}_n, \tag{4}$$

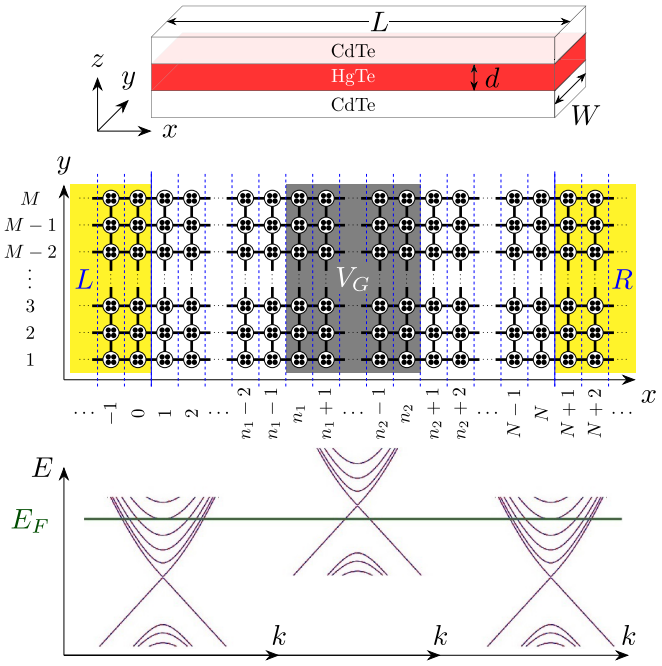

FIG. 2. Top: Sketch of the HgTe/CdTe quantum well of thickness d, width W, and length L. Middle: Sketch of the real-space discretization. N is the number of vertical slices in the central region and M is the number of sites in each slice. Each site contains four orbitals represented by black dots. The yellow shaded regions correspond to the left and right leads. The gray area represents the HgTe regions over which a gate voltage V_g is applied. Bottom: Local band structure shift due to the effect of a negative gate voltage V_g. This configuration corresponds to an n-edge-n (or n-TI-n at $B = 0$) junction.

where

$$H_{n,n}^{m,m} = \left[\mathcal{C}\mathbf{1} + \mathcal{M}\Gamma_5 - 4\frac{(\mathcal{D}\mathbf{1} + \mathcal{B}\Gamma_5)}{a^2} + \frac{\mu_B B\Gamma_g^z}{2}\right], \quad (5)$$

$$H_{n,n+1}^{m,m} = \left[\frac{(\mathcal{D}\mathbf{1} + \mathcal{B}\Gamma_5)}{a^2} + \frac{i\mathcal{A}\Gamma_1}{2a}\right] e^{ima^2(eB/\hbar)}, \quad (6)$$

$$H_{n,n}^{m,m+1} = \left[\frac{(\mathcal{D}\mathbf{1} + \mathcal{B}\Gamma_5)}{a^2} - \frac{i\mathcal{A}\Gamma_2}{2a}\right], \quad (7)$$

$$H_{n,n-1}^{m,m} = \left(H_{n,n+1}^{m,m}\right)^\dagger, \quad H_{n,n}^{m,m-1} = \left(H_{n,n}^{m,m+1}\right)^\dagger. \quad (8)$$

The above model Hamiltonian accounts for the presence of an external magnetic field perpendicular to the QW ($\mathbf{B} = B\hat{\mathbf{z}}$) by means of the gauge $\mathbf{A}(\mathbf{r}) = -By\hat{\mathbf{x}}$ and by a Zeeman term [12] $\mu_B B\Gamma_g^z/2$ where $\Gamma_g^z = \mathrm{diag}(g_e, g_h, -g_e, -g_h)$ contains the effective g-factors for electrons g_e and holes g_h and μ_B is the Bohr magneton. The Peierls phase $(e/\hbar)\int_{(n,m)}^{(n+1,m)} \mathbf{A}\cdot d\mathbf{l} = ma^2(eB/\hbar)$ modifies the hopping matrix elements between the sites (n,m) and $(n+1,m)$ in Eq. (6). Comparisons with full eight-band $\mathbf{k}\cdot\mathbf{p}$ calculations show that this low-energy model offers a good description for HgTe/CdTe QWs near the Γ point for magnetic fields up to $B \sim 2$ T [10].

We address the transport properties of a QW of thickness d, width W, and length L. The system is attached to left and right semi-infinite leads, aligned to its longitudinal direction, parallel to the x axis, as we illustrate in Fig. 2.

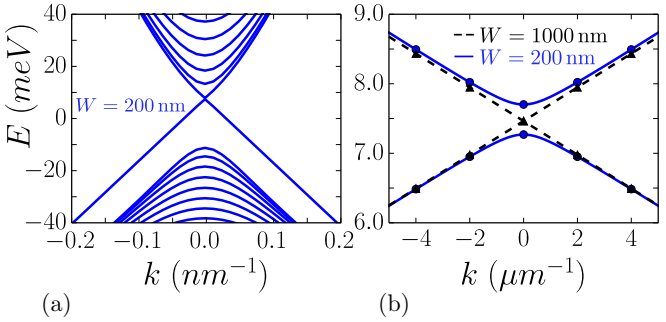

FIG. 3. (a) Spectrum of an infinite HgTe/CdTe QW of width $W = 200$ nm. (b) Detail of the edge states near $k = 0$ showing a small gap for $W = 200$ nm (blue squares) and essentially no gap for $W = 1000$ nm (black triangles). Symbols correspond to our finite differences calculation and the solid lines to analytic results of Ref. [39].

For computational convenience the QW region is divided into transverse slices that are labeled by n ranging from n_1 to n_2, see Fig. 2. We model homopolar and heteropolar junctions by introducing a gate voltage V_g acting on the system central region, corresponding to a term

$$[H_G]_{n,n}^{m,m} = eV_g\mathbf{1} \quad (9)$$

for $n_1 \leqslant n \leqslant n_2$. In this way, we approximate the model Hamiltonian of Eq. (1) by a discrete Hamiltonian on a square lattice of dimensions $M\times N$, where $W = Ma$ and $L = Na$, containing $4MN$ orbitals in the central region.

The choice of the lattice parameter a is a compromise between computational cost and accuracy. The value of a is fixed as follows: We solve the eigenproblem in Eq. (4) using periodic boundary conditions in the x direction for a chosen width W in the y direction. The reduced eigenvalue problem reads

$$E\Psi_n = \mathbf{H}_{n,n}\Psi_n + \mathbf{H}_{n,n-1}\Psi_{n-1} + \mathbf{H}_{n,n+1}\Psi_{n+1}, \quad (10)$$

where $\mathbf{H}_{n,n'}$ has the block structure $[\mathbf{H}_{n,n}]^{m,m'} = H_{n,n}^{m,m'}(\delta_{m',m} + \delta_{m',m-1} + \delta_{m',m+1})$ and $[\mathbf{H}_{n,n\pm1}]^{m,m'} = H_{n,n\pm1}^{m,m}\delta_{m',m}$. Here $H_{n,n'}^{m,m'}$ is a 4×4 matrix, given by Eqs. (5)–(8).

Due to translational invariance Ψ_n can be written as $\Psi_n = \boldsymbol{\psi}e^{ik_x na}$, where $\boldsymbol{\psi}$ has $4M$ components. For a given width W we choose a by requiring an accuracy of 10^{-2} meV in the energy gap as compared to the analytical results obtained in Ref. [39]. In practice, we fix $M = 200$ for all calculations, which sets a lattice parameter a for a given width W. We find that this procedure satisfies the required accuracy for systems with $W \lesssim 2$ μm.

Figure 3 shows valence and conduction bands of two infinite HgTe/CdTe QWs of widths $W = 200$ nm and $W = 1000$ nm obtained using the material parameters of a $d = 7$ nm thick QW [39,40] $\mathcal{A} = 364.5$ meV nm, $\mathcal{B} = -686$ meV nm^2, $\mathcal{C} = 0$, $\mathcal{D} = -512$ meV nm^2, $\mathcal{M} = -10$ meV in the absence of an external magnetic field ($B = 0$). We find that an HgTe/CdTe QW with $W = 200$ nm presents a gap of about 0.44 meV. The gap tends to close as we increase the width and reaches values as small as 10^{-5} meV for $W = 1000$ nm.

We address the charge transport properties of the HgTe/CdTe QWs using the Landauer approach [41,42]. In the

case of a vanishingly small source-drain bias, the zero temperature conductance of the system reads $G = (e^2/h)T(E_F)$, where $T(E_F) = T_\uparrow(E_F) + T_\downarrow(E_F)$ is the total transmission between the left and right contacts at the Fermi energy E_F and

$$T_\sigma(E_F) = \mathrm{Tr}\left[\Gamma_L(E_F)G^r_\sigma(E_F)\Gamma_R(E_F)G^a_\sigma(E_F)\right] \quad (11)$$

are the transmissions for each spin $\sigma = \uparrow,\downarrow$. Here G^r_σ ($G^a_\sigma = [G^r_\sigma]^\dagger$) is the retarded (advanced) Green's function for charge carriers with spin σ and Γ_L (Γ_R) is the (spin-independent) linewidth function accounting for the injection and lifetime of the carriers states in the left (right) contact.

The discrete model Hamiltonian presented above allows for a very amenable implementation of the recursive Green's functions technique [34]. We compute the linewidths Γ_L and Γ_R with standard decimation methods [43] and the full retarded Green's function G^r_σ in the system central region using the RGF [34]. We gain additional insight by computing the local transmission

$$T^\alpha_{i,j;\sigma}(E_F) = -2\mathrm{Im}\left\{\left[G^r_\sigma\Gamma_\alpha G^a_\sigma\right]_{i,j}t_{j,i}\right\} \quad (12)$$

between two neighboring states i and j connected by the hopping matrix element $t_{i,j}$ for the charge current injected from the contact $\alpha = L,R$.

III. RESULTS

In this section, we analyze the magnetotransport properties of homopolar and heteropolar junctions in HgTe/CdTe QWs by studying the local transmission of different possible double junction system configurations, namely, n-n'-n, n-TI-n (n-edge-n for $B \neq 0$), and n-p-n junctions. We present separately the analysis of the cases of $B = 0$ (Sec. III A) and $B \neq 0$ (Sec. III B).

A. Zero magnetic field

Here we study the charge transport through n-n'-n, n-TI-n, and n-p-n junctions in the presence of TRS, that is $B = 0$. As mentioned previously, we consider the case of an inverted HgTe/CdTe quantum well, $\mathcal{M} < 0$ in Eq. (1). Such systems support topologically protected edge states when TRS is preserved. Thus, the edge portion of the junction represents a topological insulator.

Let us begin by discussing the $eV_g = 0$ case, where the system is uniform. Since here the spectrum is known (e.g., Fig. 3), the current profile serves to test the accuracy of our results and to introduce the tools we use in this study.

Using Eq. (12) we calculate the stationary local left-to-right transmission between the sites i and j as $T(x_{ij},y_{ij}) \equiv |T^{\alpha=L}_{i,j;\uparrow}(E_F) + T^{\alpha=L}_{i,j;\downarrow}(E_F)|$ where (x_{ij},y_{ij}) is the midpoint between the sites. For each E_F value, we plot a color map of the normalized left-to-right transmission $\bar{T}_\sigma(x_i,y_j) \equiv (T(x_{ij},y_{ij})/T_{\max})\eta_\sigma$ where $T_{\max}$ is the maximum value of $T(x_{ij},y_{ij})$ and η_σ is the fraction of $T(x_{ij},y_{ij})$ composed by the spin $\sigma = \uparrow,\downarrow$ component. In this scheme, the values of η_σ belong to the interval $[0,1]$ satisfying $\eta_\uparrow + \eta_\downarrow = 1$. Thus, $\bar{T}_\sigma(x_i,y_j)$ for each σ varies between 0 and 1, with the unit representing full spin polarization and maximum transmission.

Typical results for $\bar{T}_\sigma(x_i,y_j)$ are shown in Fig. 4. For E_F within the gap [Fig. 4(a)], there is only a single pair of states

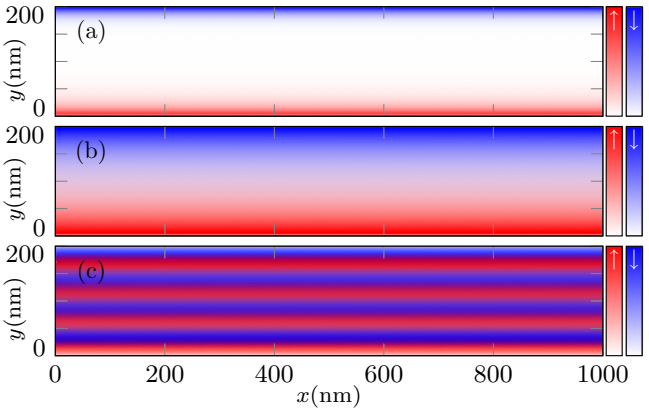

FIG. 4. Local currents in a homogeneous ($eV_g = 0$) 200×1000 nm HgTe/CdTe QW for different values of the Fermi energy E_F in the contacts, namely (a) $E_F = 0$ meV, (b) $E_F = 10$ meV, (c) $E_F = 25$ meV, and $B = 0$. Spin-polarized edge transport (from left to right) is evident for E_F inside the gap.

crossing the Fermi energy, which are localized at the QW edges. Thus, the current is carried by edge states with the expected spin texture of a topological insulator. As E_F is tuned closer to the bottom of the conduction band, the local currents still flow mostly through spin-polarized states near the edges but the contribution from bulk states become more prominent, as shown in Fig. 4(b).

In the n and p regions (E_F above and below the gap, respectively) there are well-defined spin-polarized stripes of current through the bulk. This is an interesting pattern: It implies a spatial separation of the spin-polarized currents through the bulk. This pattern originates from the different pairs of bulk and edge states crossing the Fermi level with positive group velocity, $v_k = \partial E(k)/\partial k > 0$. The helical nature of the states implies that each pair will have opposite spin polarizations. Moreover, the states in each pair are mostly symmetrically localized around the center of the strip, in opposite sides of the system, creating the pattern shown in Fig. 4(c).

We now turn to the $eV_g \neq 0$ case. Depending on the magnitude of V_g, we model a n-n'-n junction [Fig. 5(a)], a n-TI-n junction [Fig. 5(b)], or a n-p-n heteropolar junction [Fig. 5(c)]. As we discuss below, these junctions are characterized by a very distinct current density flow behavior.

Now we fix E_F at 30 meV to study n-n'-n junctions [Fig. 5(a)]. The current flow shows spin-polarized stripes across the QW transverse direction, similar to those observed for E_F outside the gap in the $eV_g = 0$ case. The situation is different in the n-p-n configuration [Fig. 5(c)]. Here, the stripe pattern in the central region seen in the n-n'-n junction vanishes due to the spatial mismatch between n-type and p-type states with positive group velocity. As a consequence of this mismatch, in the p-doped region the electronic transport is concentrated at the system edges, even though there are bulk states crossing the Fermi energy.

The n-TI-n configuration [Fig. 5(b)] shows a spatial filtering, where the current flows through spin-polarized edge states. Interestingly, reflections at the n-edge interface create a snakelike pattern for the spin-polarized currents.

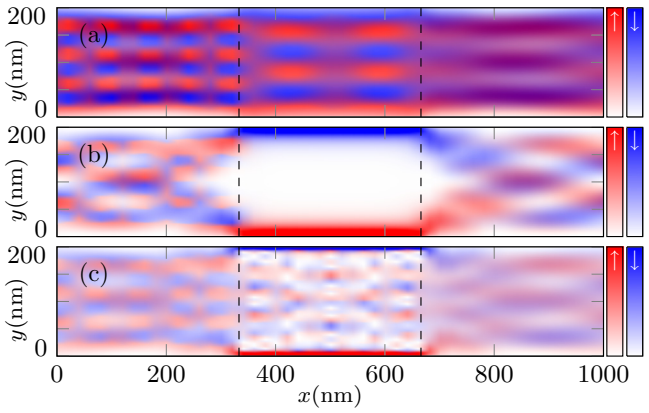

FIG. 5. Local currents in different junctions: (a) n-n'-n (b) n-TI-n, and (c) n-p-n junctions. In all cases, we considered a 200×1000 nm HgTe/CdTe QW and $B = 0$. The gate voltage in the central region was held, respectively at (a) $eV_g = 10$ meV (b) $eV_g = 30$ meV and (c) $eV_g = 60$ meV. The E_F in the contacts was set to 30 meV from the bottom of the valence band. Notice the edge-dominated transport in the n-TI-n junction, for which E_F is set inside the gap in the central region.

This is better illustrated by Fig. 6, where the spin-up component of the transmission near the interface is shown for clarity. As previously discussed, in the TI region the spin-up current is localized at the bottom edge. This behavior becomes increasingly clear as one moves away from the interface. Figure 6 also shows a strong downward flow of spin-up electrons parallel to the interface, represented by the (blue) vertical arrow. Spin-up electron injected in the upper part of the junction cannot propagate the TI region and move along snakelike trajectories along the interface [36,37], which channels the flow towards the system bottom edge.

On the n-doped side of the junction the behavior is strikingly different. The spin-up electrons flow alternates in direction along the system transversal direction. As above, the bottom edge states also contribute to the left-right current in the

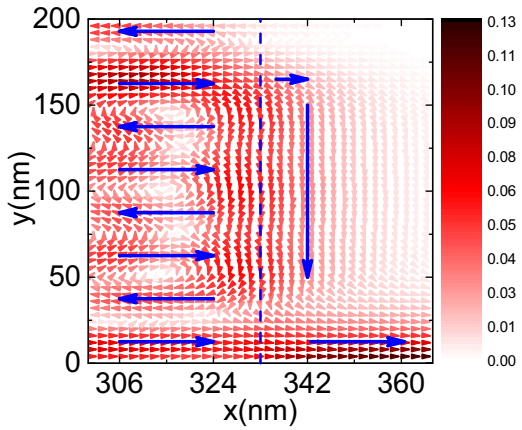

FIG. 6. Detail of the spin up current along the interface in an n-TI junction, showing a snakelike pattern in the n side (left) of the junction. In the TI side (right), the spin-up electrons flow parallel to the interface to the bottom edge state, where the left-right transmission across the junction takes place.

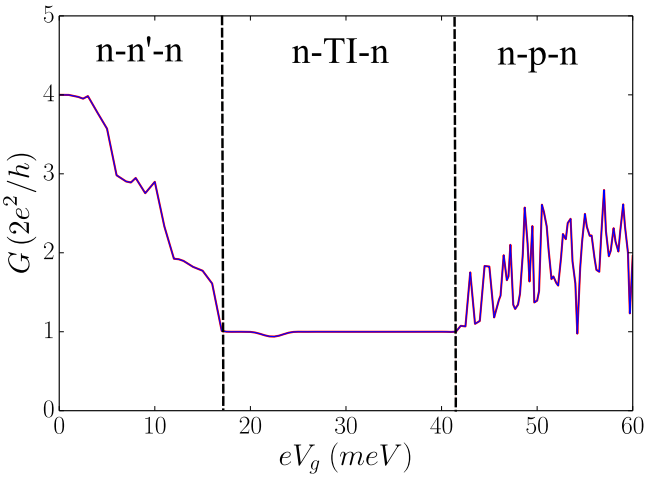

FIG. 7. Landauer conductance as a function of eV_g for a 200×1000 nm HgTe/CdTe ribbon for $B = 0$. Transport in the n-n'-n shows plateaus, with small oscillations, while the n-TI-n region is characterized by a clear $2e^2/h$ plateau. The little bump at $\approx$22.5 meV signals a small gap in the spectrum shown in Fig. 3. Strong oscillations in the n-p-n region occur due to the mismatch of the wave functions in n and p regions.

n-region, producing a strong left-to-right spin-up component matching the flux on the TI side. By contrast, the contribution from bulk states is either (i) reflected at the interface, producing small vortexlike patterns and a backward flow, or (ii) injected in the TI region in the upper section and then channeled downward along the interface. The combination of these two effects produces the current pattern in the n-doped region indicated by the (blue) horizontal arrows in Fig. 6.

This picture allows us to interpret the conductance in these systems. Figure 7 shows the conductance per spin as a function of the gate voltage V_g. The conductance plateaus in the n-n'-n region essentially count the number of open modes at the Fermi energy in the central region for a given V_g. As V_g is tuned so that the E_F lies inside the gap, a clear $2e^2/h$ plateau appears. A small depression in the transmission near $eV_g \approx 22.5$ meV signals the presence of a finite-size gap in the spectrum. The gap is small enough so that the effective broadening arising from the coupling of the system to the contacts (which is captured by the RGF approach) is sufficient to give a large contribution to the transmission at that energy value. In the n-p-n region, the conductance oscillates rapidly with V_g. This is a result of the multiple reflections and the wave mismatch between n and p regions. Note that the states with positive group velocity, that contribute to the left-to-right charge flow, have opposite phase velocity in n and p regions, which enhance the mismatch between those states.

B. Transport at nonzero field

We now study the transport properties of HgTe QW junctions under an external perpendicular magnetic field B. We consider QWs of $W = 200$ nm. In this case, the transition to a regime where transport is dominated by quantum-Hall-like chiral edge modes occurs at $B_c \approx 7$–8 T [14]. Thus, we restrict

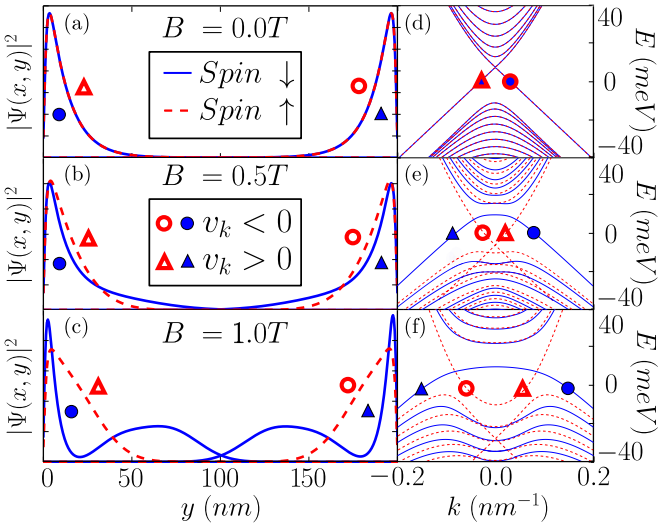

FIG. 8. Wave functions for states inside the bulk gap for $L =$ 200 nm and (a) $B = 0$, (b) 0.5, and (c) 1.0 T for different k_x values, as marked on the corresponding dispersion relations (d)–(f). As B increases, the spin-up states remain localized close to the edge, while the spin-down states move toward the bulk. The resulting hybridization opens a gap in the spin-down spectrum. Red dashed (blue solid) lines represent spin-up (spin-down) states. Backward- ($v_k < 0$) and forward-moving ($v_k > 0$) states are marked by circles and triangles, respectively. Solid (open) symbols represent spin-down (spin-up) states.

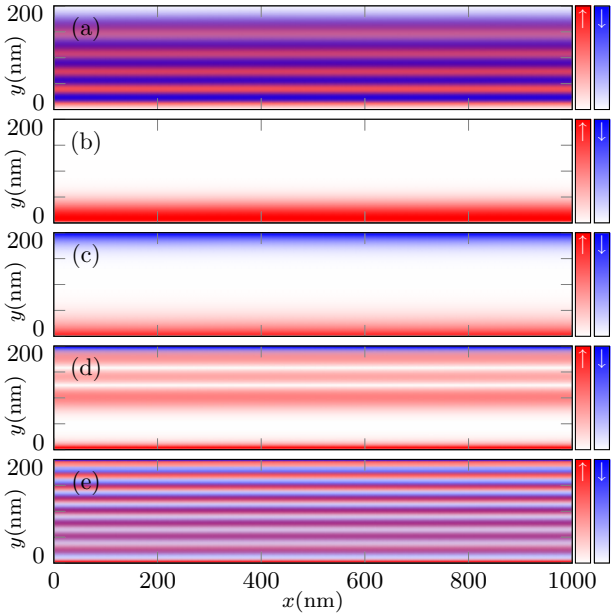

FIG. 9. Local currents for an homogeneous ($eV_g = 0$) 200×1000 nm HgTe/CdTe QW subjected to a perpendicular magnetic field at $B = 0.5$T. The currents are shown for different values of the Fermi energy E_F in the contacts, namely (a) 40 meV (n-type transport), (b) 15 meV, (c) 5 meV, (d) −16 meV, and (e) −40 meV (p-type transport) (see Fig. 3).

our analysis to B fields up to 2T, where counterpropagating helical states are still present in the system.

As it is well known [1–3], a magnetic field breaks TRS and thus the edge states lose their topological protection. Moreover, the Zeeman term in Eq. (1), although small, also breaks the spin degeneracy. The combination of these two effects substantially changes the spin-dependent transport properties across the junction.

We begin by exploring the nonzero B case for the $eV_g = 0$ case. Figure 8 contrasts the probability distributions of the system states at $E_F = 0$ and the dispersion relations for representative values of B. Consistent with previous studies [13], for $B = 0.5$T, a well-pronounced gap (∼10 meV) appears for spin-down states, while the spin-up states show no gap. As the field increases, the probability density of the spin-up states remains concentrated at the edges, while the spin-down states penetrate deeper into the bulk. This behavior is consistent with the local currents shown in Figs. 9(b)–9(d) for selected values of the Fermi energy. In those cases, the asymmetry with respect to the y axis (across the width) appears because only the forward-moving states at one edge are present in the transport.

For n- and p-type transport, Figs. 9(a) and 9(e), respectively, the bulk currents flow along nearly spin-polarized stripes, similarly to the $B = 0$ case. However, some interesting differences appear. When the Fermi energy lies inside the spin-down gap, the current is fully spin-up polarized, flowing through the lower edge [Fig. 9(b)]. As E_F is tuned slightly below the spin-up gap, the system shows spin-polarized transport on both edges, similar to the topological case, as shown in Fig. 9(c). Note that the threshold for spin-up bulk states is higher in energy than the spin-down states, leading to a region where we have transport dominated by bulk spin-up and edge spin-down currents Fig. 9(d).

We now consider the local currents in HgTe n-(central)-n junctions at a finite magnetic field. Figure 10 shows the behavior for different values of V_g such that E_F lies close to the spin-down local gap in the central region. Figures 10(a) and 10(e) correspond to n-n'-n and n-p-n junctions, respectively. In these cases the transport properties are dominated by bulk states and orbital interference effects.

When E_F lies within the spin-down gap, a spin-up polarized current flows through the lower edge of the central region [Fig. 10(b)] and it is injected in the right n region through an edge state. A slight increase in eV_g (from 20–22.5 meV) is sufficient to bring E_F to cross the first spin-down edge state below the gap, thereby allowing spin-down transport through the upper edge of the central region [Fig. 10(c)].

Surprisingly, a further small increase in eV_g (from 22.5–25 meV) causes the spin down current in the central region to practically vanish, as shown in Fig. 10(d). This is at odds with the homogeneous case (Fig. 9) where spin-down currents are always present as long as E_F lies outside the spin-down gap. We attribute this suppression to the large change in momentum across the n-edge junction necessary for the propagation of spin-down electrons in the central region, as inferred from the band structure in Fig. 8(e).

Let us now examine the conductance across the junction as a function of the gate voltage V_g for $B = 0.5$ T. Figure 11 shows a clear oscillatory pattern of the spin-down current for $eV_g >$ 20 meV up to the onset of n-p-n behavior at $eV_g \approx 40$ meV. In

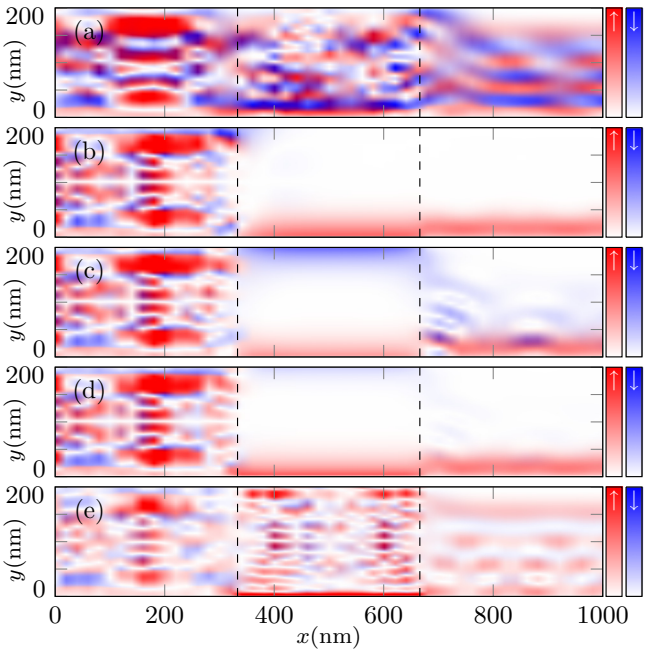

FIG. 10. Local currents for a n-(central region)-n junction in a 200×1000 nm HgTe/CdTe QW, with $B = 0.5$T and $E_F = 30$ meV for different eV_g values, namely (a) -10 meV (n-n'-n junction), (b) 20 meV, (c) 22.5 meV, (d) 25 meV, and (e) 60 meV (n-p-n junction).

the same V_g range, the spin-up conductance remains at a e^2/h plateau, indicating spin-polarized edge transmission for the V_g values where the spin-down current essentially vanishes.

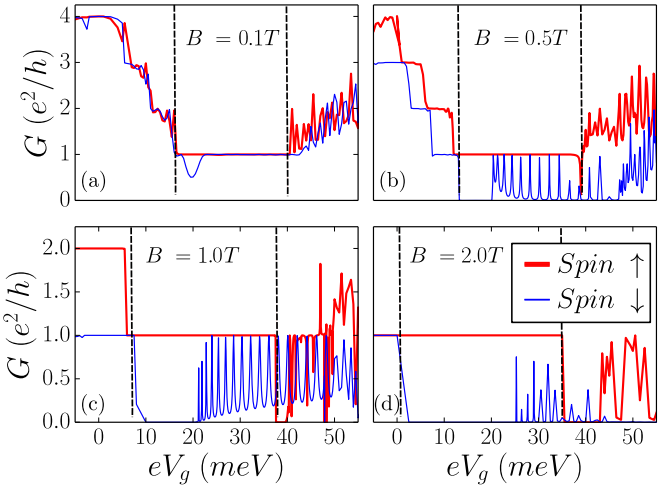

FIG. 11. Conductance per spin versus V_g for different values of the magnetic field. The eV_g range sweeps the junction from n-n'-n ($eV_g = 10$ meV) to n-p-n ($eV_g = 60$ meV). For weak fields, the currents are nearly spin independent, with a $2e^2/h$ plateau due to edge state transport. A gap in the spin-down spectrum becomes more prominent for larger fields. For $B = 0.5$ T, a clear oscillatory pattern (on/off) in the spin-down current appears between the spin gap edge ($eV_g = 20$ meV) and the onset of n-p-n behavior ($eV_g \approx 40$ meV). Notice that this edge current behavior extends to fields as large as $B = 2$ T, (d).

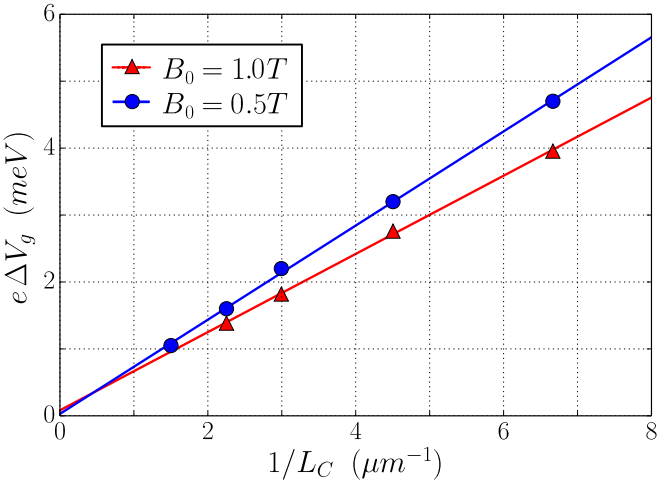

FIG. 12. Spin-down transmission peak spacing versus $1/L_C$ (L_C is the central region length) for different magnetic field values. The $1/L_C$ scaling in all cases is consistent with Fabry-Pérot-like oscillations due to backscattering via reflection with the step potential at the junction interface.

We associate these peaks with Fabry-Pérot resonances caused by backscattering at the junction interfaces. Figure 12 shows that the spacing ΔV_g between the transmission peaks displays a linear scaling with the inverse of the central region length L_C, indicating single-particle interference due to backscattering at the interfaces. Similar phenomena has been investigated previously in two-terminal devices in the presence of a magnetic field [11,44]. Here, the presence of the interfaces magnifies the effect, leading to strong oscillations where a perfect spin-polarized transport across the junction is possible.

Fabry-Pérot-like oscillations also appear for larger magnetic field values and are suppressed for lower ones. In fact, the oscillations seem to occur only in the presence of a fully developed gap in the spin-down spectrum, as shown in Figs. 11(b) and 11(c).

For $B = 2$T, Fig. 11(d), the behavior is similar. Since the spin-down gap is significantly larger, the range of V_g for which the current displays full spin-up polarization increases from $eV_g \approx 12.5$–20 meV for $B = 0.5$ T to $eV_g \approx 5$–25 meV for $B = 2$ T. Interestingly, for larger V_g values ($eV_g \gtrsim 35$ meV), spin-up drops to zero and full spin-down polarization is now possible. Thus, for these moderate magnetic field values, the junction operates as a gate-tunable spin polarization switch.

IV. CONCLUDING REMARKS

In this paper we have theoretically studied the spin-dependent local currents in HgTe/CdTe quantum-well monopolar and heteropolar junctions. We considered the dependence of the transport properties with an applied magnetic field perpendicular to the sample and the resulting transition from topologically protected edge transport to a regime where spin backscattering is allowed at the junction barriers.

For zero magnetic field, our recursive Green's functions calculations for the local currents show distinct characteristics for n-n'-n, n-TI-n and n-p-n junctions. While the bulk

contributions to the current are strong in monopolar (n-n'-n) junctions, in the heteropolar case transport is dominated by edge states in the central region. In n-TI-n junctions, the spin-resolved flow alternates in direction along the system transverse direction in the n side of the first n-TI interface. By contrast, the TI side shows currents flowing parallel to the interface toward the edges, where the main flow occurs.

Edge states still give a strong contribution to the transmission in the presence of TRS-breaking perpendicular magnetic field. Interestingly, the magnetic field opens a gap for one of the spins. Quantum interference due to backscattering at the interface produces spin-resolved Fabry-Pérot-like oscillations in the transmission as a function of the gate applied to the central region.

The combination of the gap opening and the Fabry-Pérot oscillations for only one of the spins allows for the production of tunable spin-polarized currents across the junction for moderate ($B < 1$ T) values of the magnetic field. We stress that these results are generic for other inverted QWs displaying 2D topological insulator behavior such as InAs/GaSb [45,46]. This opens the prospect for applications of inverted QW heteropolar junctions in spintronic devices.

ACKNOWLEDGMENTS

D.N. and L.R.F.L. acknowledge support from the Brazilian funding agencies CNPq, FAPERJ and CAPES. L.D.S. acknowledges support from CNPq Grants No. 307107/2013-2 and No. 449148/2014-9, and FAPESP Grant No. 2016/18495-4, and PRP-USP NAP-QNano. C.H.L. is supported by CNPq Grant No. 308801/2015-6 and FAPERJ Grant No. E-26/202.917/2015.

[1] M. Z. Hasan and C. L. Kane, Rev. Mod. Phys. **82**, 3045 (2010).
[2] X.-L. Qi and S.-C. Zhang, Rev. Mod. Phys. **83**, 1057 (2011).
[3] Y. Ando, J. Phys. Soc. Jpn. **82**, 102001 (2013).
[4] C. L. Kane and E. J. Mele, Phys. Rev. Lett. **95**, 146802 (2005).
[5] B. A. Bernevig, T. L. Hughes, and S.-C. Zhang, Science **314**, 1757 (2006).
[6] M. Konig, S. Wiedmann, C. Brune, A. Roth, H. Buhmann, L. W. Molenkamp, X.-L. Qi, and S.-C. Zhang, Science **318**, 766 (2007).
[7] J. Maciejko, X.-L. Qi, and S.-C. Zhang, Phys. Rev. B **82**, 155310 (2010).
[8] A. Mani and C. Benjamin, J. Phys.: Condens. Matter **28**, 145303 (2016).
[9] A. Mani and C. Benjamin, Phys. Rev. Appl. **6**, 014003 (2016).
[10] M. J. Schmidt, E. G. Novik, M. Kindermann, and B. Trauzettel, Phys. Rev. B **79**, 241306 (2009).
[11] G. Tkachov and E. M. Hankiewicz, Phys. Rev. Lett. **104**, 166803 (2010).
[12] B. Buttner, C. X. Liu, G. Tkachov, E. G. Novik, C. Brune, H. Buhmann, E. M. Hankiewicz, P. Recher, B. Trauzettel, S. C. Zhang, and L. W. Molenkamp, Nat. Phys. **7**, 418 (2011).
[13] J.-c. Chen, J. Wang, and Q.-f. Sun, Phys. Rev. B **85**, 125401 (2012).
[14] B. Scharf, A. Matos-Abiague, and J. Fabian, Phys. Rev. B **86**, 075418 (2012).
[15] O. E. Raichev, Phys. Rev. B **85**, 045310 (2012).
[16] M. V. Durnev and S. A. Tarasenko, Phys. Rev. B **93**, 075434 (2016).
[17] G. M. Gusev, Z. D. Kvon, O. A. Shegai, N. N. Mikhailov, S. A. Dvoretsky, and J. C. Portal, Phys. Rev. B **84**, 121302 (2011).
[18] G. M. Gusev, E. B. Olshanetsky, Z. D. Kvon, N. N. Mikhailov, and S. A. Dvoretsky, Phys. Rev. B **87**, 081311 (2013).
[19] G. M. Gusev, A. D. Levin, Z. D. Kvon, N. N. Mikhailov, and S. A. Dvoretsky, Phys. Rev. Lett. **110**, 076805 (2013).
[20] S. Essert and K. Richter, 2D Mater. **2**, 024005 (2015).
[21] J. Martin, N. Akerman, G. Ulbricht, T. Lohmann, J. H. Smet, K. von Klitzing, and A. Yacoby, Nat. Phys. **4**, 144 (2008).
[22] E. R. Mucciolo and C. H. Lewenkopf, J. Phys.: Condens. Matter **22**, 273201 (2010).
[23] S. Das Sarma, S. Adam, E. H. Hwang, and E. Rossi, Rev. Mod. Phys. **83**, 407 (2011).
[24] V. V. Cheianov, V. I. Fal'ko, B. L. Altshuler, and I. L. Aleiner, Phys. Rev. Lett. **99**, 176801 (2007).
[25] L. R. F. Lima and C. H. Lewenkopf, Phys. Rev. B **93**, 045404 (2016).
[26] Z. Fan, A. Uppstu, and A. Harju, 2D Mater. **4**, 025004 (2017).
[27] L. B. Zhang, K. Chang, X. C. Xie, H. Buhmann, and L. W. Molenkamp, New J. Phys. **12**, 083058 (2010).
[28] L. B. Zhang, F. Zhai, and K. Chang, Phys. Rev. B **81**, 235323 (2010).
[29] L. B. Zhang, F. Cheng, F. Zhai, and K. Chang, Phys. Rev. B **83**, 081402 (2011).
[30] S. U. Piatrusha, V. S. Khrapai, Z. D. Kvon, N. N. Mikhailov, S. A. Dvoretsky, and E. S. Tikhonov, arXiv:1703.09816.
[31] M. R. Calvo, F. de Juan, R. Ilan, E. J. Fox, A. J. Bestwick, M. Muhlbauer, J. Wang, C. Ames, P. Leubner, C. Brune, S. C. Zhang, H. Buhmann, L. W. Molenkamp, and D. Goldhaber-Gordon, arXiv:1702.08561.
[32] D. A. Abanin and L. S. Levitov, Science **317**, 641 (2007).
[33] J. R. Williams, L. DiCarlo, and C. M. Marcus, Science **317**, 638 (2007).
[34] C. H. Lewenkopf and E. R. Mucciolo, J. Comp. Electron. **12**, 203 (2013).
[35] B. Scharf, A. Matos-Abiague, I. Žutić, and J. Fabian, Phys. Rev. B **91**, 235433 (2015).
[36] P. Carmier, C. Lewenkopf, and D. Ullmo, Phys. Rev. B **81**, 241406 (2010).
[37] P. Carmier, C. Lewenkopf, and D. Ullmo, Phys. Rev. B **84**, 195428 (2011).
[38] Moreover, Rashba spin-orbit coupling is expected to give only a minor contribution to the transport in the quasi-1D regime [28].
[39] B. Zhou, H.-Z. Lu, R.-L. Chu, S.-Q. Shen, and Q. Niu, Phys. Rev. Lett. **101**, 246807 (2008).
[40] M. Konig, H. Buhmann, L. W. Molenkamp, T. Hughes, C.-X. Liu, X.-L. Qi, and S.-C. Zhang, J. Phys. Soc. Jpn. **77**, 031007 (2008).
[41] S. Datta, *Electronic Transport in Mesoscopic Systems* (Cambridge University Press, Cambridge, 1997).
[42] H. Haug and A. J. Jauho, *Quantum Kinetics in Transport and Optics of Semiconductors*, Solid-State Sciences, Vol. 123 (Springer, Heidelberg, 2008).

[43] M. P. L. Sancho, J. M. L. Sancho, and J. Rubio, J. Phys. F: Met. Phys. **15**, 851 (1985).

[44] A. Soori, S. Das, and S. Rao, Phys. Rev. B **86**, 125312 (2012).

[45] L. Du, I. Knez, G. Sullivan, and R.-R. Du, Phys. Rev. Lett. **114**, 096802 (2015).

[46] M. Karalic, C. Mittag, T. Tschirky, W. Wegscheider, K. Ensslin, and T. Ihn, Phys. Rev. Lett. **118**, 206801 (2017).